Self-Organizing Control for Space-Based Sparse Antennas

Fred Y. Hadaegh, Vaharaz Jamnejad, Daniel P. Scharf, and Scott R. Ploen

Jet Propulsion Laboratory
California of Institute of Technology
Pasadena, CA 91109 USA
Hadaegh@jpl.nasa.gov

Abstract

An integrated control and electromagnetic/antenna formulation is presented for evaluating the performance of a distributed antenna system as a function of formation geometry. A distributed and self-organizing control law for the control of multiple antennas in Low Earth Orbit (LEO) is presented. The control system provides collaborative commanding and performance optimization to configure and operate the distributed formation system. A large aperture antenna is thereby realized by a collection of miniature sparse antennas in formation. A case study consisting of a simulation of four antennas in Low Earth Orbit (LEO) is presented to demonstrate the concept.
Keywords: Formation flying, Leader/Follower, Self-organizing, Sparse antenna, Formation control

1. Introduction

In recent years, the science community has been actively considering the use of distributed spacecraft for deep space and Earth science missions. One such application is to use a large number of small spacecraft in place of a large deployable antenna in order to achieve very large sparse apertures for Earth imaging (for example, at resolutions of ≈ 10 cm). Another application is the use of multiple telescopes flying in precision formation as an interferometer in deep space for stellar imaging and planet detection. A number of such missions have been proposed that offer unprecedented performance capabilities beyond the scope of any single large telescope [17,18]. Compared to their equivalent monolithic aperture counterparts, formation flying sparse antennas offer launch and deployment efficiency, and has the advantage of avoiding the structural complexity and pointing issues associated with large aperture, lightweight, antenna dishes in space.

This paper presents an integrated control and electromagnetic/antenna approach needed to realize, for the first time, distributed formation flying spacecraft antenna systems in Low Earth Orbit (LEO). The paper focuses on the core guidance and control (G&C) algorithms needed to perform parametric studies to access the impact of replacing a large monolithic space-based antenna by a collection of miniature spacecraft. This concept is shown in Figure 1. The development of techniques/algorithms to couple formation flying with 3-dimensional electromagnetic field pattern generation is another important objective of this paper. To this end, formation dynamics and environmental disturbance modeling is presented in Section 3. Formation guidance and control design for both translation and attitude are presented in Section 4 and 5. Section 6 provides analysis of a spatial array of antennas along with simulations. Section 7 presents a four-spacecraft sparse aperture example for evaluation of the distributed antenna system performance.

Figure 1. Can a few small antennas replace a larger antenna in space?

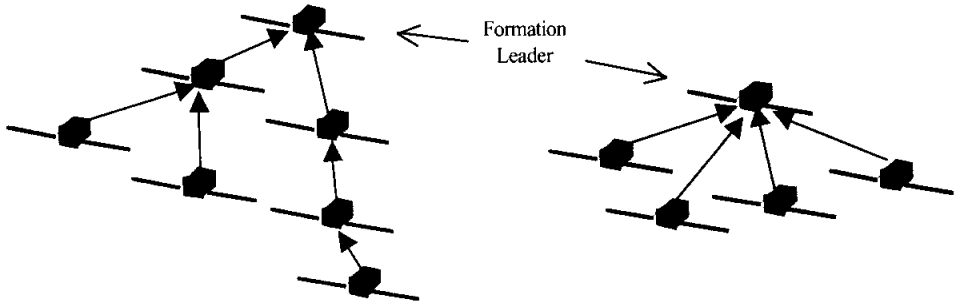

Figure 2. Two possible L/F architectures. Solid arrows indicate leader assignment.

2. Sparse Antenna Guidance and Control Architecture

In general, the methodology for coordination and control of spacecraft in a formation is strongly correlated with the formation size and particular application. In a completely centralized architecture, a single master spacecraft commands all aspects of the other slave spacecraft. At the other end of the spectrum is a completely decentralized architecture in which spacecraft interact locally with other nearby spacecraft. In this latter case, formation behavior is said to be "emergent," and is similar to the schooling of fish or the flocking of birds. The defining characteristic of a decentralized architecture is that individual spacecraft do not require knowledge of the entire formation state for control.

Here we use the Leader/Follower (L/F) decentralized control architecture [8] for controlling relative spacecraft *positions* (attitude control is discussed subsequently). This architecture is robust and scaleable (e.g., individual spacecraft failures do not affect the overall formation stability and additional spacecraft can be easily added using only local control design[1]). In the L/F architecture, individual spacecraft controllers are connected in a hierarchical fashion. With the exception of the formation leader discussed below, each spacecraft is assigned a leader that the spacecraft "follows," i.e., a follower spacecraft controls its position with respect to its leader. The leader may in turn be following another spacecraft. There is at least one spacecraft in the formation that does not follow another spacecraft. This spacecraft is referred to as the formation leader. The motion of the formation leader controls the motion of the entire formation. We initially consider small to medium formations (i.e., 5 to 10 spacecraft). In this case, a single-layer L/F architecture is feasible. Hence, all spacecraft follow the same spacecraft, which is the designated formation leader. For larger formations, single-layer L/F imposes restrictive inter-spacecraft communication and sensing requirements. Figure 2 shows examples of a general L/F architecture and a single-layer L/F architecture.

Absolute spacecraft attitudes are controlled independently so that individual apertures are pointed in the nadir direction.[2] A spacecraft's nadir direction is determined using real time inertial position knowledge obtainable from GPS measurements to 10 m(1σ) accuracy (we cannot use precision centimeter level orbit determination as was used for Topex/Poseidon since this position data is delayed by up to a day) [9]. For the orbits considered, a 10 m inertial positioning error leads to a maximum nadir pointing error of 0.1 arc-minutes. Therefore, inertial positioning errors can be ignored for our purposes.[3]

The formation guidance has a hybrid architecture; part centralized and part decentralized. The attitude guidance is decentralized; each spacecraft points its aperture in the nadir direction independently of the other spacecraft. The translational guidance is centralized. A path-planning algorithm on the formation leader plans the relative trajectories of each follower with respect to the formation leader. These trajectories are then communicated to the followers.

For a collection of spacecraft (apertures) to function cooperatively as a sparse antenna, the control system must be capable of maintaining specified relative

[1] To add or remove a spacecraft from a centralized formation control architecture, the entire formation controller must be redesigned.

[2] Another alternative to be evaluated is using L/F to point all spacecraft in the formation leader's nadir direction.

[3] GPS-based technologies are being developed that can sense inertial positions to the centimeter level in real time. These technologies have the capability of superceding carrier differential GPS-based measurements in the future.

spacecraft positions to a fraction of the antenna wavelength. As a result, scientific applications require *precision formation flying* (i.e., centimeter/arc-minute-level relative position/attitude control). Relative position requirements have been previously studied for synthetic aperture applications: In the VHF radio frequency band (i.e., 1 to 10 m wavelengths), relative spacecraft positions must be controlled to approximately the 15 cm level. Similarly, for interferometric synthetic aperture radar applications in the L band (15 to 30 cm wavelengths), relative spacecraft positions must be controlled to approximately the 3 cm level [1]. These relative positioning requirements are consistent with current carrier differential phase GPS (CDGPS) sensors, which can measure relative positions with 2 cm (1σ) of accuracy. Attitude requirements for radar and radio frequency synthetic apertures are not as well defined [2]; a spacecraft must only point to a fraction of an aperture's beam pattern width [3], which is application dependent.

In this paper, we assume that all the spacecraft are nadir-pointing (i.e., down-looking) and that the attitude control requirements are consistent with attitude sensing via CDGPS (i.e., 5 to 10 arcminute level)[10].

In summary, robust precision formation control and guidance algorithms must be developed that (1) maintain relative spacecraft positions and absolute attitudes to 5 cm and 10 arc-minutes, respectively, and that (2) reconfigure the formation using fuel-optimal, collision free trajectories. Further, these algorithms must perform over orbits with altitudes ranging from 250 to 1000 km and non-zero eccentricity.

3. Formation and Environmental Disturbance Models

A sparse antenna formation may be in a circular 200 km or an eccentric 1000 km orbit. The ambient formation dynamic environment varies widely over this range of possible orbits. For example, the relative spacecraft dynamics are time-invariant (to first order) for a circular orbit, but are time-varying for an eccentric orbit. Further, disturbances vary by orders of magnitude depending upon orbit semi-major axis and inclination. In the following section, the equations of motion for an N spacecraft formation of distributed antennas in LEO are presented followed by models for environmental disturbances.

3.1 Distributed Antennas Models

Each antenna is modeled as a rigid body with three translational and three rotational degrees-of-freedom. Each spacecraft is subjected to a pure Keplerian (i.e., two-body) gravitational potential along with environmental disturbances including perturbations due to J_2 oblateness effects, aerodynamic drag, solar radiation pressure, and Sun/Moon gravitational perturbations. We further assume that each spacecraft has full control authority in both translation and rotation along all axes. The orbital geometry of the formation is shown in Figure 3. Here the translational motion of spacecraft i relative to spacecraft j is described with respect to a Keplerian reference orbit where $\vec{R}_O$ denotes the reference orbit trajectory, and $\vec{\rho}_i$ denotes the position of the i^{th} spacecraft relative to the origin of the orbit reference frame. The linearized translational equations of motion of each spacecraft $i = 1,2,\ldots N$ valid for $|\vec{\rho}_i| << |\vec{R}_o|$ are given by

$$\ddot{\vec{R}}_O + \frac{\mu \vec{R}_O}{R_O^3} = \vec{0} \tag{1}$$

$$\ddot{\vec{\rho}}_i + \frac{\mu}{R_O^3}\left(\vec{I} - 3\hat{o}_1 \otimes \hat{o}_1\right)\vec{\rho}_i = \vec{a}_{oi} + \vec{a}_{pi} + \frac{1}{m_i}\left(\vec{F}_{ai} + \vec{F}_{si} + \vec{F}_{ci}\right) \tag{2}$$

Here the magnitude of $\vec{R}_O$ is denoted by R_O, $\{\hat{o}_1, \hat{o}_2, \hat{o}_3\}$ denotes the right-handed orthonormal triad defining the orbit reference frame shown in Figure 3 where $\hat{o}_1$ points nadir, $\hat{o}_2$ is normal to the plane of the reference orbit, and $\hat{o}_3$ completes the triad, μ denotes the gravitational parameter of the Earth, $\vec{I}$ denotes the unit dyadic, the symbol $\otimes$ denotes the tensor product, $\vec{a}_{oi}$ denotes the perturbation on the i^{th} spacecraft due to central-body oblateness effects, $\vec{a}_{pi}$ denotes the perturbation on the i^{th} spacecraft due to the gravitational attraction of the Sun and Moon, $\vec{F}_{ai}$ is the resultant aerodynamic force at the center-of-mass of the i^{th} spacecraft, $\vec{F}_{si}$ is the resultant solar radiation force acting at the center-of-mass of the i^{th} spacecraft, and $\vec{F}_{ci}$ denotes the control force applied to the center-of-mass of the i^{th} spacecraft. Note that all derivatives in the equations of motion are inertial derivatives.

The rotational equations of motion of each antenna $i = 1,2,\ldots N$ are given by

$$\dot{q}_i = \frac{1}{2}\Gamma(q_i)\vec{\omega}_i \tag{3}$$

$$\vec{J}_i\dot{\vec{\omega}}_i + [\vec{\omega}_i]\vec{J}_i\vec{\omega}_i = \vec{\tau}_{ai} + \vec{\tau}_{si} + \vec{\tau}_{ci} \tag{4}$$

where q_i denotes the unit quaternion describing the absolute attitude of the i^{th} spacecraft, Γ is the attitude dependent kinematic Jacobian matrix, $\vec{\omega}_i$ denotes the absolute angular velocity of the i^{th} spacecraft, $[\vec{\omega}_i]$ denotes the skew-symmetric cross product operator, $\vec{J}_i$ denotes the central inertia dyadic of the i^{th} spacecraft, $\vec{\tau}_{ai}$ denotes the resultant aerodynamic torque acting at the center-of-mass of the i^{th} spacecraft, $\vec{\tau}_{si}$ denotes the resultant solar radiation torque acting at the center-of-mass of the i^{th} spacecraft, and $\vec{\tau}_{ci}$ denotes the applied control torques at the center-of-mass of the i^{th} spacecraft.

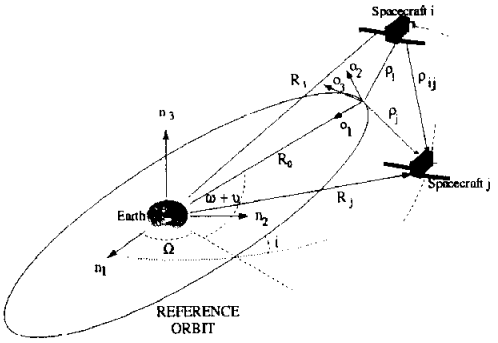

Figure 3. Orbital Geometry

3.2 Environmental Disturbance Models

In this section, the explicit form of the disturbance models appearing in the equations of motion are presented. First, the perturbation due to Earth oblateness effects on the i^{th} spacecraft is given by

$$\vec{a}_{oi} = -\frac{3\mu J_2 a^2}{2R_i^4}(c_{1i}\hat{e}_i + c_{2i}\hat{n}_3) \tag{5}$$

where $c_{1i} = 1 - 5(\hat{e}_i \bullet \hat{n}_3)^2$, $c_{2i} = 2(\hat{e}_i \bullet \hat{n}_3)$, and the symbol $\bullet$ denotes the standard dot product. Also J_2 denotes the second zonal harmonic of the Earth, a is the mean radius of the Earth, $\hat{e}_i$ denotes a unit vector along the absolute position vector $\vec{R}_i$ of spacecraft i, R_i denotes the magnitude of $\vec{R}_i$, and $\hat{n}_3$ denotes the polar axis of the Earth. Note that the perturbation due to oblateness has components in both the radial and polar directions.

The perturbations on the i^{th} spacecraft due to third-body (e.g., Sun, Moon) gravitational interactions is given by

$$\vec{a}_{pi} = \sum_{j=1}^{N_p} \mu_j \left(\frac{\vec{r}_{1j} - \vec{R}_i}{r_{2j}^3} - \frac{\vec{r}_{1j}}{r_{1j}^3} \right) \tag{6}$$

where μ_j is the gravitational parameter of the j^{th} perturbing body, N_p denotes the number of perturbing bodies and the vectors $\vec{r}_{1j}$ and $\vec{r}_{2j}$ are as shown in Figure 4.

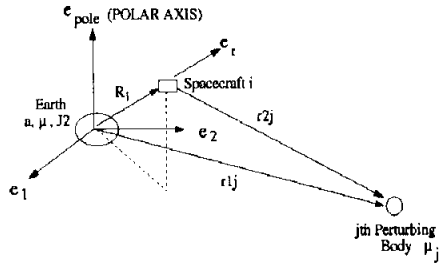

Figure 4. Geometry of Third-body Perturbations

The aerodynamic disturbances acting on a single spacecraft are modeled by approximating each spacecraft as a convex collection of flat faces. For simplicity we assume that all spacecraft are identical and consist of the same number of faces, denoted N_{face}. The resultant aerodynamic force and torque about the center of mass of the i^{th} spacecraft, denoted $\vec{F}_{ai}$ and $\vec{\tau}_{ai}$ respectively, are given by

$$\vec{F}_{ai} = \sum_{j=1}^{N_{face}} \eta_j \vec{F}_{a,ij} \tag{7}$$

$$\vec{\tau}_{ai} = \sum_{j=1}^{N_{face}} \eta_j \vec{r}_{ij} \times \vec{F}_{a,ij} \tag{8}$$

where

$$\vec{F}_{aij} = -\frac{1}{2} C_{d,ij} A_{ij} \rho V_{rel,ij}^2 (\hat{n}_{ij} \bullet \hat{V}_{rel,ij}) \hat{V}_{rel,ij} \tag{9}$$

and

$$\vec{V}_{rel,ij} = (\vec{V}_i + \vec{\omega}_i \times \vec{r}_{ij}) - \vec{\omega}_p \times (\vec{R}_i + \vec{r}_{ij}) \tag{10}$$

Here $\vec{F}_{a,ij}$ denotes the resultant aerodynamic force acting on the j^{th} face of the i^{th} spacecraft, $\vec{r}_{ij}$ is the center-of-mass to center-of-pressure offset of the j^{th} face of the i^{th} spacecraft, η_j denotes a face participation factor, $C_{d,ij}$ denotes the drag coefficient of the j^{th} face of spacecraft i, A_{ij} denotes the area of the j^{th} face of the i^{th} spacecraft, ρ is the altitude-dependent atmospheric density, $\hat{n}_{ij}$ denotes the unit normal of the j^{th} face of the i^{th} spacecraft, $\vec{V}_{rel,ij}$ is the velocity of the j^{th} face of the i^{th} spacecraft relative to the atmosphere, $\hat{V}_{rel,ij}$ denotes a unit vector along $\vec{V}_{rel,ij}$, $\vec{V}_i$ is the absolute velocity of the center-of-mass of the i^{th} spacecraft, $\vec{\omega}_i$

denotes the absolute angular velocity of spacecraft i, $\vec{R}_i$ is the absolute position of the center-of-mass of the i^{th} spacecraft, and $\vec{\omega}_p$ denotes the absolute angular velocity of the Earth. Note that we have assumed the atmosphere rotates with the same angular velocity as the Earth.

The disturbance due to solar radiation pressure acting on a single spacecraft is also computed by approximating each spacecraft as a collection of flat faces. The resultant force and torque about the center of mass of the i^{th} spacecraft due to solar radiation pressure, denoted $\vec{F}_{si}$ and $\vec{\tau}_{si}$ respectively, are given by

$$\vec{F}_{si} = \sum_{j=1}^{N_{face}} \eta_j \vec{F}_{s,ij} \quad (11)$$

$$\vec{\tau}_{si} = \sum_{j=1}^{N_{face}} \eta_j \vec{r}_{ij} \times \vec{F}_{s,ij} \quad (12)$$

where

$$F_{s,ij} = -PA_{ij}(\hat{n}_{ij} \bullet \hat{s}_{ij})[(1-c_{s,ij})\hat{s}_{ij} + 2\{c_{s,ij}(\hat{n}_{ij} \bullet \hat{s}_{ij}) + \frac{1}{3}c_{d,ij}\}\hat{n}_{ij}] \quad (13)$$

Here $\hat{s}_{ij}$ denotes a unit vector from the center-of-mass of the j^{th} face of the i^{th} spacecraft to the Sun, P denotes the mean momentum flux at 1AU, $c_{s,ij}$ is the coefficient of specular reflection of the j^{th} face of the i^{th} spacecraft, and $c_{d,ij}$ is the coefficient of diffuse reflection of face j of the i^{th} spacecraft.

4. Formation Guidance Design

The formation guidance algorithm has two functions: (1) planning relative positions of the follower spacecraft so that the desired electromagnetic beam pattern is attained, and (2) planning fuel-optimal, collision-free reconfiguration trajectories to form new beam patterns or balance fuel consumption. The first guidance function requires optimal aperture positioning (a genetic-algorithm based approach is presently under study), and a prescribed set of relative spacecraft positions is used for this purpose.

The second guidance function has been designed and implemented using two different algorithms. The first algorithm is applicable to formations in circular orbits, and is based on linearized Lambert targeting (LLT) using the Hill-Clohessy-Wiltshire (HCW) equations discussed below. The collision avoidance algorithm for LLT guidance is heuristic-based, and is not guaranteed to converge to collision-free trajectories nor is it optimal. However, the LLT algorithm is a quick and efficient method for calculating reconfigurations. The second reconfiguration guidance algorithm is an implementation of the linear programming (LP) algorithm of [15]. The LP algorithm is applicable to formations in eccentric orbits. However, it is optimal only when the fleet leader is fixed on a reference orbit. The LP algorithm first discretizes the control input and then minimizes the absolute value of the acceleration for a spacecraft reconfiguration. For our purposes, the main benefit of the LP algorithm is the ability to enforce state constraints for collision avoidance.

5. Formation Control Design

5.1. Translational Control

Since our primary goal is to develop a general formation controller to support sparse aperture beam pattern analysis/optimization over a wide range of formation orbits, a classical design method was chosen for developing the individual spacecraft translational control-laws. Classical design methods have straightforward robustness criteria and have proven to perform adequately even when design assumptions are violated. The control design-model is based on the HCW equations, which describe the relative (linearized) translational dynamics between a leader and follower spacecraft when they are near a circular orbit. The reference frame and variables used in the HCW equations are shown in Figure 5. The HCW frame has an origin O traveling on a circular reference orbit and coordinate axes $\hat{x}_h, \hat{y}_h$, and $\hat{z}_h$ where $\hat{y}_h$ is parallel to the circular orbit velocity, $\hat{z}_h$ is perpendicular to the orbital plane, and $\hat{x}_h$ completes the right-handed triad. The HCW frame is also rotating with constant angular velocity $\vec{\omega}_0 = \omega_0 \hat{z}_h$. The position of the leader in the HCW frame is given by $\vec{\rho}_j$ and the position of the follower by $\vec{\rho}_i$. The position of the leader with respect to the follower, resolved in the HCW frame, is given by $\rho_{ij} = [x \quad y \quad z]^T$. When both $|\vec{\rho}_j|$ and $|\vec{\rho}_i|$ are small compared to the orbital radius, the equations of motion are

$$\ddot{x} - 3\omega_0^2 x - 2\omega_0 \dot{y} = a_x \quad (14)$$

$$\ddot{y} + 2\omega_o \dot{x} = a_y \quad (15)$$

$$\ddot{z} + \omega_o^2 z = a_z \quad (16)$$

where a_x, a_y and a_z are inertial accelerations due to all control forces and disturbances resolved in the HCW frame.

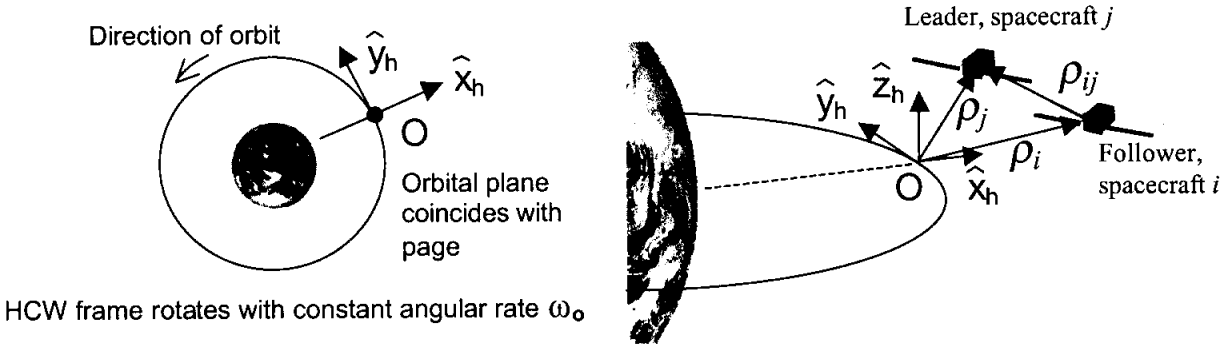

Figure 5. HCW Frame and Variables used in the HCW Equations

In the HCW equations, the x and y motion is coupled, and the z motion is decoupled. As a result, the z motion controller can be designed using standard single-input, single output (SISO) classical design methods. However, the combined x and y motion constitutes a multiple-input, multiple-output (MIMO) system, and so classical MIMO design methods must be used.

There are a variety of classical MIMO design techniques, but generally they first attempt to make a MIMO system look approximately SISO, and then apply SISO design methods [12,13]. We adopt the sequential loop closure MIMO technique, illustrated in Figure 6. This technique generates a diagonal MIMO controller in the frequency domain of the form

$$K(s)=\begin{bmatrix} K_1(s) & 0 \\ 0 & K_2(s) \end{bmatrix} \tag{17}$$

by only considering unidirectional (i.e., hierarchical) MIMO coupling during the initial control design. After an initial controller has been obtained, the control design is iterated with full bi-directional coupling to guarantee stability.

A representative single loop control design (e.g., the z motion control loop or the $K_1(s)G_{11}(s)$ loop in Figure 6) is shown in Figures 7 and 8. Figure 7 is the Bode diagram for the representative loop transfer function. The ω_0 resonance at 2×10^{-4} Hz which is proportional to the reciprocal of the reference orbit period is apparent. Note that since the control is implemented at 1 Hz, the Bode plot only extends to 0.5 Hz.

Figure 8 shows the loop frequency response (solid line) in the L-plane (i.e., magnitude in dB versus phase in degrees). The frequency response must remain outside the dark dashed box for the standard stability margins of 6 dB and 30 degrees. The light dashed lines indicate the conditional stability boundaries (i.e., if the frequency response remains below and to the right of the green lines, then control

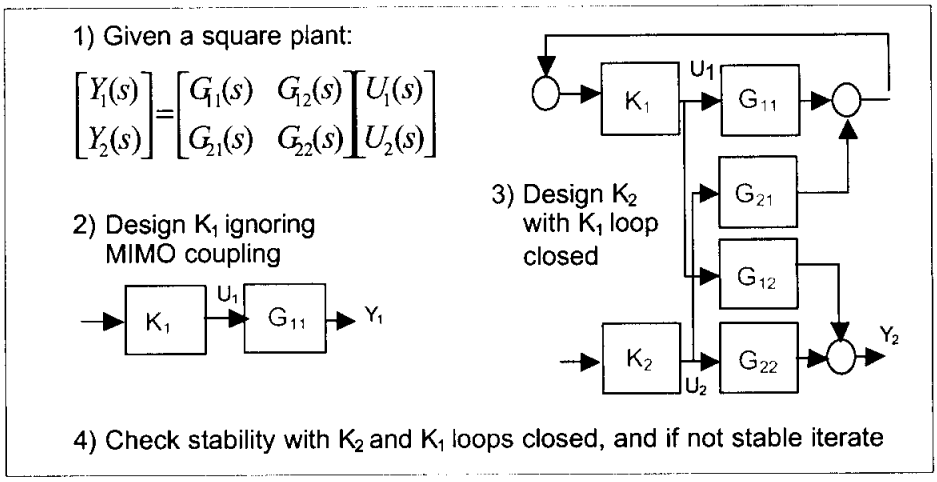

Figure 6. Sequential Loop Closure Design Technique

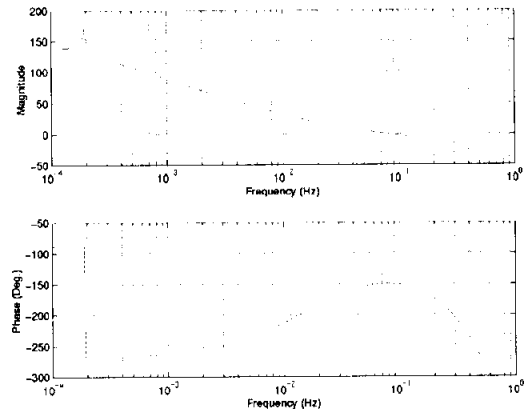

Figure 7. Bode Diagram of Representative Controller Loop Transfer Function

saturation will not necessarily destabilize the controller). To obtain increased control performance, the translational controller was designed to be conditionally stable.

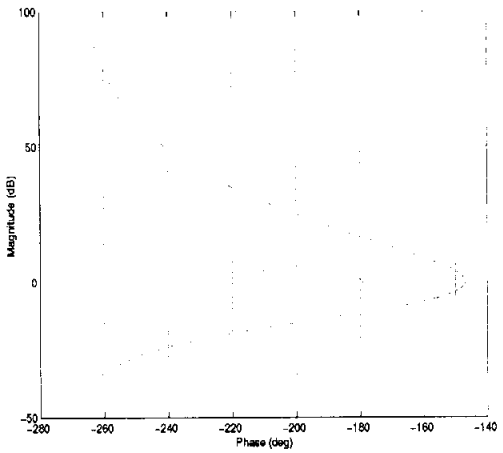

Figure 8. L-Plane Diagram of Representative Controller Loop Transfer Function

The MIMO translational control design was evaluated using the high-fidelity, nonlinear "truth" model developed in Section 3. A follower spacecraft was given a 1 m step command with respect to the leader. The resulting error time histories are shown in Figure 9. The leader is in a 0.05 eccentric orbit, *which violates the circular assumption* of the HCW equations used for controller design. Note, however, that the closed-loop system is still stable. There is significant y-motion overshoot due mainly to the sequential loop closure design technique (bi-lateral coupling was ignored in the design of the y loop). In practice, the controller will not see a 1 m step, and so the absolute tracking performance during reconfigurations (when performance requirements are relaxed) will be considerably less. Future work would also involve designing a pre-compensator to reduce overshoot.

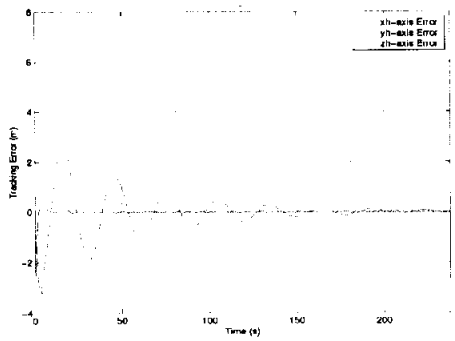

Figure 9. Follower Relative Position Error

The translational controller was also evaluated for its precision performance. Assuming 2 cm (1σ) sensor noise and a 0.05 eccentricity reference orbit, the position of a follower with respect to the leader was maintained constant to within 3 cm (1σ) in each axis. All the control loops are type 1 or better, so that quasi-static disturbances such as aerodynamic drag can be rejected. Finally, the bandwidth of each loop is approximately 0.08 Hz.

The translational control design meets the 5 cm precision requirement discussed earlier, and it is robust to the entire range of formation orbits being considered in this paper.

5.2 Attitude Control

The attitude control design model is based on Euler's equations (i.e. the balance of angular momentum) linearized about the Local-Vertical-Local-Horizontal (LVLH) frame. The LVLH frame travels on a circular orbit and rotates with the circular orbit just as the HCW frame does. In particular, the LVLH frame rotates with constant angular velocity $\vec{\omega}_{orbit} = -\omega_0 \hat{y}_L$, where ω_0 is the same as in the HCW equations. However, the LVLH frame is rotated with respect to the HCW frame so that the $\hat{z}_L$ coordinate axis points in the nadir direction. See Figure 10.

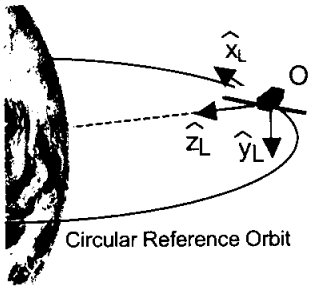

Figure 10. Local-Vertical-Local-Horizontal Frame

The angular deviations in each axis are given by ε_{xL}, ε_{yL} and ε_{zL}, respectively. An "L" subscript has been included to indicate the LVLH frame as opposed to the HCW frame. The resulting attitude dynamics are then

$$I_x\ddot{\varepsilon}_{xL} + (I_y - I_z)\omega_O^2\varepsilon_{xL} + (I_y - I_x - I_z)\omega_O\dot{\varepsilon}_{zL} = \tau_x \quad (18)$$

$$I_z\ddot{\varepsilon}_{zL} + (I_y - I_x)\omega_O^2\varepsilon_{zL} + (I_x + I_z - I_y)\omega_O\dot{\varepsilon}_{xL} = \tau_z \quad (19)$$

$$I_y\ddot{\varepsilon}_{yL} = \tau_y \quad (20)$$

where I_x, I_y and I_z are the principal moments of inertia about the spacecraft center of mass, and τ_x, τ_y, and τ_z denote the control and disturbance torques resolved in the LVLH frame. Two implicit assumptions in Equations (18)-(20) are that the principal axes of the spacecraft coincide with the body frame and that the body frame coincides with the LVLH frame when the attitude control error is zero.

Note that Equations (18) and (19) are coupled, whereas (20) is decoupled. This structure is identical to the structure of the translational control design model given in Equations (14)-(16). Although, in this case the $\hat{x}_L$ and $\hat{z}_L$ motions are coupled. Since the design process is essentially the same, we only report the results of the attitude control design.

Figure 11 shows the angular deviations (errors) as a function of time for an attitude test case. Again, the full, nonlinear equations of motion have been used to validate the controller designed on the simplified dynamics (18) – (20). The spacecraft is originally aligned with the HCW frame. It is then commanded to slew to align with the LVLH frame. This maneuver represents a "worst case" large-angle slew that would be used to point the apertures after deployment or a recovery from a fault condition. Note that the controller is stable even though the small angle assumption is violated.

The attitude controller loop transfer function shapes are very similar to those of the relative translational controller show in Figures 7 and 8. Further, the attitude controller is also discretized at 1 Hz, and the control bandwidths are approximately 0.08 Hz in each axis. Assuming 6 arcminute (1σ) sensor noise and a 0.05 eccentricity reference orbit, the attitude was maintained constant to within 8 arcmintues (1σ) in each axis. Therefore, the attitude controller meets the 10 arcminute performance requirement over the entire range of formation orbits considered.

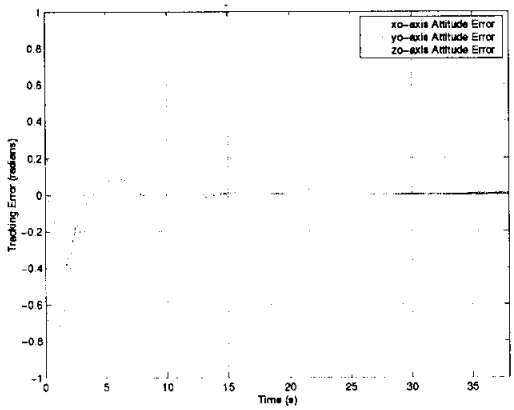

Figure 11. Attitude Controller Evaluation

6. Analysis of a Spatial Array of Aperture Antennas

An array of small aperture antennas on multiple spacecraft can be synthesized into a single antenna whose properties are determined by the characteristics of each individual antenna and their respective excitation phases and amplitudes. Such a composite antenna has definite advantages in terms of deployment flexibility. Specifically, as individual spacecraft are launched separately, the deployment of an individual antenna (spacecraft) consisting of a small solid one-piece aperture, is much more reliable and less subject to failure. Furthermore, the surface tolerances of these individual small apertures can be maintained with a high degree of accuracy.

This distributed antenna arrangement provides for the independent active control of each sub-aperture in terms of its phase and amplitude. Therefore, by independent mechanical and electrical RF control of each element, the composite antenna can be reconfigured for different RF properties such as beamwidth, and the beam can be scanned electronically (e.g., in a phased array the direction of maximum gain can be changed without changing the orientation of the individual apertures). This

arrangement also provides flexibility in dividing the array into two or more separate sub-arrays with distinct individual beams and applications. The distributed array provides graceful performance degradation in case of a single or a few individual aperture/spacecraft failures. The ability to add new antennas/spacecraft as needed is another advantage of such an arrangement.

6.1 Various geometrical arrangements of the arrays

There are many possible arrangements of the elements of an array, each requiring separate analysis techniques. Although each element can be a different type of antenna with different characteristics and parameters, in most applications they are identical. Furthermore, the antennas are generally assumed to have the same physical and pattern orientation (i.e., all the beams of individual antennas are in the same direction and have identical field polarization). We have developed a suite of MATLAB programs that can analyze general array cases, which include most of the above arrangements as special cases. Specifically, the general analysis of a planar array of regularly spaced *identical elements* with *identical orientations* has been developed in simulation using both closed-form analytical solutions as well as numerical integration. Individual elements can have different power and phase. Further, the analysis of a general three-dimensional array of *identical elements,* each with *different orientations* and *arbitrary general spatial locations* (to account for the tolerances in position and orientation), has also been developed for pattern and gain calculation using numerical integration.

6.2 Array Formulation

The geometry of the array is shown Figure 12. Two cases are considered. First a general array of identical elements with arbitrary locations in space and arbitrary orientations is formulated. The results are then specialized for the case of a planar array of elements with identical orientations. This results in a substantial simplification, and for certain types of elements, leads to a closed-form solution for the gain of the array.

6.3 MATLAB Implementation

In the first implementation we employed the full cosine pattern for element pattern representation. Both analytical closed-form solutions as well as a numerical integration method were utilized. The input to the program includes the position of each element in space and the orientation of the array. In its present form, the program calculates the peak gain of the array, and plots pattern cuts corresponding to ϕ=0 deg. (x-z plane), ϕ=90 deg. (y-z plane), or any other specified azimuth angle ϕ. In addition, three-dimensional plots and contour plots of the beam pattern in u-v space, where $u=sin(\theta)cos(\phi)$, $v=u=sin(\theta)sin(\phi)$, and θ denotes the co-latitude are provided. In the final implementation of the program, a general three-dimensional array of elements with arbitrary locations and orientations were considered. Full cosine, as well as half-cosine and lambda element pattern representations, were included. The input to the program includes the location of each element in space as well as the Eulerian angles describing its orientation. The program calculates the peak gain of array, and plots pattern cuts corresponding to any specified azimuth angle ϕ. In addition three-dimensional plots as well as contour plots of the beam pattern in u-v space are provided. As an example, the beam contour plots in u-v space of a two-element array ($x = \pm 1\lambda$, where λ is the wavelength) with variations of element positions in x, y, and z directions are shown in Figure 13.

7. G&C Simulation Architecture

An integrated guidance and control simulation testbed was developed that allows direct visualization of the coupling between orbital motion and the three-dimensional (spatial) antenna array pattern. The testbed was used to perform computer simulations to study the dynamic behavior of the distributed antenna formations, and assess the performance of the separated spacecraft antenna system. The G&C algorithms described above have been integrated with the electromagnetic/antenna field computations to analyze a formation of N distributed antennas in LEO. The geometric and mass properties of the spacecraft can be varied. The simulation architecture has blocks for formation estimation, guidance and control. Different formation scenarios are addressed by modifying the formation guidance blocks in each of the spacecraft. An inertial vector propagator is used to update the nadir direction and there are also blocks for mode commanding and thrust allocation. Currently, inter-spacecraft communication is assumed ideal (i.e., no delays). See Figures 14 and 15.

8. Conclusion

This paper introduced modeling, and G&C methodologies for a set of antennas flying in formation in LEO. The electromagnetic/antenna performance of a distributed and self-organizing formation was evaluated through a control system that achieved collaborative commanding and performance optimization to configure and operate

the distributed formation system. A case of four antennas in Low Earth Orbit (LEO) was presented and it was shown that proper configuration and orbital positioning of antennas could lead to unprecedented antenna system performance capability.

The simultaneous control and coordination of individual spacecraft is a very complicated task. Specifically, maintaining precision position and attitude tolerances while coordinating RF excitations for various elements in a spatially separated environment is a non-trivial task. These areas must be studied in greater detail to provide feasible implementation techniques.

Acknowledgments
The work described in this paper was carried out at the Jet Propulsion Laboratory, California Institute of Technology, under contract with the National Aeronautics and Space Administration.

References
[1] Goodman, N.A., Lin, S.C., Rajakrishna, D., and Stiles, J.M., "Processing of Multiple-Receiver Spacecbourne Arrays for Wide-Area SAR," *IEEE Trans. Geoscience and Remote Sensing*, Vol. 40(4), pp. 841-852, 2002.
[2] Corazzini, T., Robertson, A., Adams, J.C., Hassibi, A., and How, J.P., "Experimental Demonstration of GPS as a Relative Sensor for Formation Flying Spacecraft," *J. of the Institute of Navigation*, Vol. 45(3), pp. 195-207, 1998.
[3] Moccia, A., and Vetrella, S., "A Tethered Interferometric Synthetic Aperture Radar (SAR) for a Topographic Mission," *IEEE Trans. Geoscience and Remote Sensing*, Vol. 30(1), pp. 103-109, 1992.
[4] Zebker, H.A., Farr, T.G., Salazar, R.P., and Dixon, T.H., "Mapping the World's Topography Using Radar Interferometry: The TOPSAT Mission," *Proc. of the IEEE*, Vol. 82(12), pp. 1774-1786, 1994.
[5] Massonnet, D., "Capabilities and Limitations of the Interferometric Cartwheel," *IEEE Trans. Geoscience and Remote Sensing*, Vol. 39(3), pp. 506-520, 2001.
[6] Crassidis, J.L., Lightsey, E.G., and Markley, F.L., "Efficient and Optimal Attitude Determination Using Recursive Global Positioning System Signal Operation," *J. Guidance, Control, and Dynamics*, Vol. 22(2), pp. 193-201, 1999.
[7] Oshman, Y., and Markley, F.L., "Spacecraft Attitude/Rate Estimation Using Vector-Aided GPS Observations," *IEEE Trans. Aerospace and Electronic Systems*, Vol. 35(3), pp. 1019-1032, 1999.
[8] Wang, P.K.C., and Hadaegh, F.Y., "Coordination and Control of Multiple Microspacecraft Moving in Formation," *J. of the Astronautical Sci.*, Vol. 44(3), pp. 315-355, 1996.
[9] Bauer, F.H., Hartman, K., and Lightsey, E.G., "Spacebourne GPS Current Status and Future Visions," *IEEE Aerospace Conf.*, 1998.
[10] Crassidis, J.L., Lightsey, E.G., and Markley, F.L., "Efficient and Optimal Attitude Determination Using Recursive Global Positioning System Signal Operation," *J. Guidance, Control, and Dynamics*, Vol. 22 (2), pp. 193-201, 199.
[10] Crassidis, J.L., Lightsey, E.G., and Markley, F.L., "Efficient and Optimal Attitude Determination Using Recursive Global Positioning System Signal Operation," *J. Guidance, Control, and Dynamics*, Vol. 22 (2), pp. 193-201, 199.
[11] Haines, B.J., Lichten, S.M., Lough, M.F., Muellerschoen, R.J., and Vigue-Rodi, Y., "Determining Precise Orbits for Topex/Poseidon within One Day of Real Time: Results and Implications," *AAS/AIAA Spaceflight Mechanics Meeting*, pp. 623-634, 1999.
[12] Maciejowski, J.M., Multivariable Feedback Design, Addison-Wesley Publishing Company: Wokingham, England, 1989.
[13] Hovd, M., Braatz, R.D., and Skogestad, S., "SVD Controllers for H_2-, H_8- and μ-Optimal Control," *American Control Conf.*, 1994.
[14] Prussing, J.E., and Conway, B.A., Orbital Mechanics, Oxford University Press: New York, 1993.
[15] Tillerson, M., Inalhan, G., and How, J.P., "Co-ordination and Control of Distributed Spacecraft Systems Using Convex Optimization Techniques," *Int. J. of Robust and Nonlinear Control*, Vol. 12, pp. 207-242, 2002.
[16] Singh, G. and Hadaegh, F.Y., "Collision Avoidance Guidance for Formation-Flying Applications," *AIAA Guidance, Navigation, and Control Conf.*, 2001.
[17] Gendreau, K.C., White, N., Owens, S., Cash, W., Shipley, A., and Joy, M., "The MAXIM X-ray Interferometry Mission Concept Study," *36th Liege Int. Astrophysics Colloquium*, Liege, Belgium, 2001.
[18] Beichman, C.A., "The Terrestrial Planet Finder: The Search for Life-Bearing Planets Around Other Stars," *SPIE Conference on Astronomical Interferometry*, Kona, Hawaii, 1998.

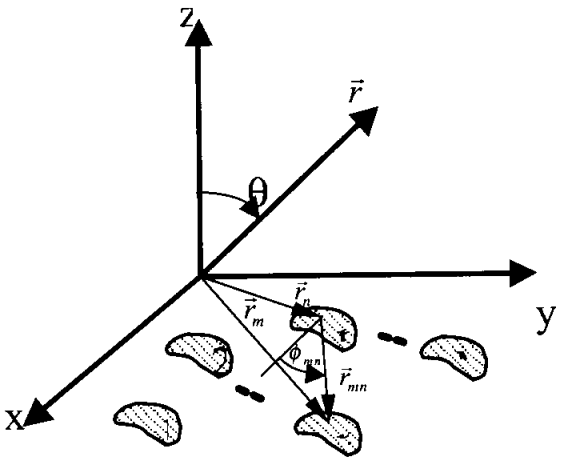

Figure 12. Sparse antenna geometry

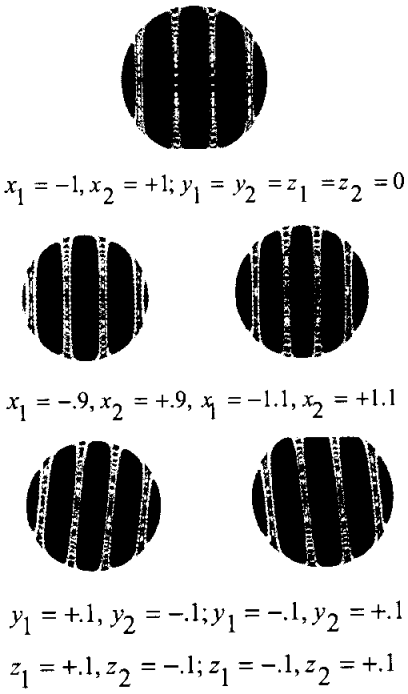

Figure 13. Beam Contour Variations

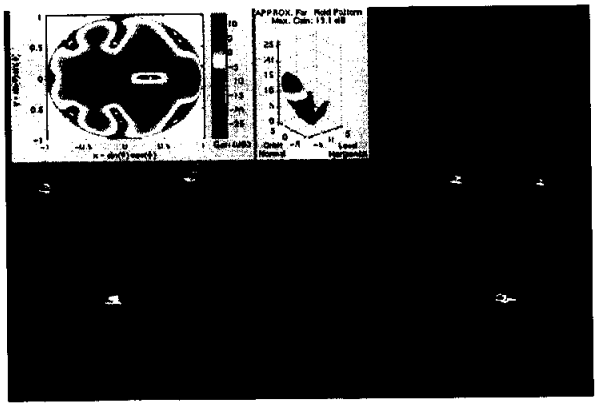

Figure 14. Simulation testbed GUI

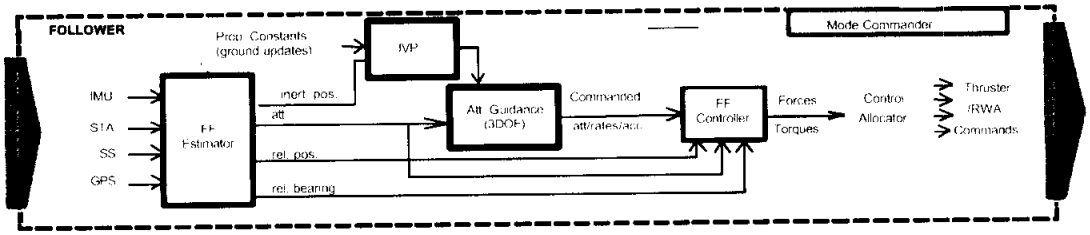

Figure 15. Formation G&C architecture